

Near-infrared light propagation in an adult head model. II. Effect of superficial tissue thickness on the sensitivity of the near-infrared spectroscopy signal

Eiji Okada and David T. Delpy

It is important for near-infrared spectroscopy (NIRS) and imaging to estimate the sensitivity of the detected signal to the change in hemoglobin that results from brain activation and the volume of tissue interrogated for a specific source–detector fiber spacing. In this study light propagation in adult head models is predicted by Monte Carlo simulation to investigate the effect of the superficial tissue thickness on the partial optical path length in the brain and on the spatial sensitivity profile. In the case of source–detector spacing of 30 mm, the partial optical path length depends mainly on the depth of the inner skull surface whereas the spatial sensitivity profile is significantly affected by the thickness of the cerebrospinal fluid layer. The mean optical path length that can be measured by time-resolved experiments increases when the skull thickness increases whereas the partial mean optical path length in the brain decreases when the skull thickness increases. These results indicate that it is not appropriate to use the mean optical path length as an alternative to the partial optical path length to compensate the NIRS signal for the difference in sensitivity caused by variation of the superficial tissue thickness.

© 2003 Optical Society of America

OCIS codes: 170.0170, 170.3660, 170.3890.

1. Introduction

Near-infrared spectroscopy (NIRS) and imaging has been applied to measure brain activation noninvasively. NIRS^{1,2} is widely used to monitor the change in blood volume and oxygenation in the brain, and the development of commercial instruments has enabled routine brain monitoring. A multichannel system for topographic imaging can also obtain a topographical distribution of the activated region in the brain cortex by a simple mapping algorithm.^{3–5} In brain activation measurements by NIRS and topographic imaging, the source and detector fibers are attached to the scalp with incident light penetrating the brain and being scattered back through the scalp. Since

absorption of the activated region varies by changes in the blood volume and oxygenation, one can measure brain activation by detecting the intensity change of near-infrared light that passes through the brain.

The fundamental and serious problem of NIRS and imaging is ambiguity in light propagation in the head caused by the scattering of biological tissue. This poses difficulties in the quantification of NIRS and results in poor spatial resolution and contrast in the near-infrared images. It is clinically important to know the sensitivity of the detected signal to the absorption change in the brain and the volume of tissue interrogated with a particular source–detector pair. Although these clinically important parameters cannot be obtained directly by experiments, the partial optical path length in the brain⁶ and the spatial sensitivity profiles⁷ can be predicted by numerical analysis of light propagation in the head as indices of the sensitivity and volume of tissue interrogated. The light that passes into the brain must pass through superficial tissues such as the scalp and the skull, and hence the thickness and the structure of these superficial tissues obviously affect the near-infrared measurements.

E. Okada (okada@elec.keio.ac.jp) is with the Department of Electronics and Electrical Engineering, Keio University, 3-14-1 Hiyoshi, Kohoku-ku, Yokohama 223-8522, Japan. D. T. Delpy is with the Department of Medical Physics and Bioengineering, University College London, 11-20 Capper Street, London WC1E 6JA, United Kingdom.

Received 13 September 2002.

0003-6935/03/162915-08\$15.00/0

© 2003 Optical Society of America

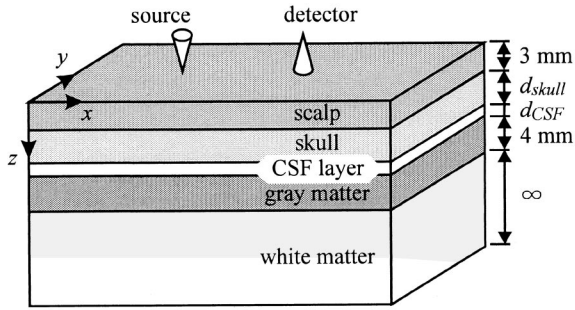


Fig. 1. Adult head model used to evaluate the effects of superficial tissues on light propagation in the brain.

In this study, the effect of the superficial tissue thickness of the head on the sensitivity of the detected near-infrared signal and the volume of tissue interrogated with a source–detector pair is investigated. We focus on the effects of the skull and cerebrospinal fluid (CSF) layer including arachnoid trabeculae although the superficial tissues in reality consist of the scalp, skull, dura mater, arachnoid mater, CSF layer, and pia mater. Light propagation in the brain is strongly affected by the presence of the low-scattering CSF layer,^{8–14} and the thickness of the CSF is easily varied because the brain can move or expand to a limited degree within the skull. The thickness of the skull is known to vary significantly around the head and between individuals. It is likely that the effect of the skull and CSF on the sensitivity and volume of tissue interrogated is quite different because the scattering coefficient of the CSF layer is considerably lower than that of the skull. Here we predict light propagation in adult head models including skull and CSF layers of various thicknesses by Monte Carlo simulation to obtain information about the partial optical path length in the brain and the spatial sensitivity profile as well as the detected intensity and total mean optical path length. The latter two parameters can be measured experimentally if needed.

2. Method for Modeling Light Propagation

A. Adult Head Model

The adult head model is a slab that consists of five layers that imitate the scalp, skull, CSF layer, gray

Table 1. Thickness and Optical Properties for Each Layer of an Adult Head Model

Tissue Type	Thickness (mm)	Transport Scattering Coefficient μ_s' (mm^{-1})	Absorption Coefficient μ_a (mm^{-1})
Scalp	3.0	1.9	0.018
Skull	4.0–12.0	1.6	0.016
CSF layer	0.25–5.0	0.24	0.004
Gray matter	4.0	2.2	0.036
White matter	—	9.1	0.014

matter, and white matter as shown in Fig. 1. The optical properties of the layers for near-infrared light of 800-nm wavelength shown in Table 1 were chosen from reported data^{15–17} except for those of the CSF layer. To our knowledge, there are no experimental data on the optical properties of the CSF layer as yet and hence we estimate them from our previous results.¹⁸ The low level of scattering in the CSF layer was assumed to arise from the arachnoid trabeculae. The thickness of the scalp and the cortical gray matter for all the models were 3 and 4 mm. The thickness of the skull was altered progressively from 4 to 12 mm with the CSF thickness held constant at 2 mm to evaluate the effect of the skull thickness on the light propagation in an adult head. Similarly the CSF layer thickness was altered from 0.25 to 5 mm but with the skull thickness held constant at 7 mm to evaluate the effect of the CSF layer thickness on the light propagation in an adult head.

B. Monte Carlo Simulation

The NIRS signal ΔOD , which is the change in intensity of the detected light, is given by¹⁹

$$\Delta OD = \Delta \ln(I_0/I) \approx \Delta \mu_a \text{head} \langle L_{\text{head}} \rangle, \quad (1)$$

where I_0 is the incident light intensity, I is the intensity of the detected light, $\Delta \mu_a \text{head}$ is the apparent absorption change in the head under the assumption that the absorption changes homogeneously in the head, and $\langle L_{\text{head}} \rangle$ is the mean optical path length. The mean optical path length can be measured by time- or phase-resolved instrumentation. However, the assumption of a homogeneous head is obviously not realistic.

The NIRS signal can also be obtained from the change in absorption $\Delta \mu_a i$ and the partial optical path length $\langle L_i \rangle$ in layer i as follows⁸:

$$\begin{aligned} \Delta OD \approx & \Delta \mu_a \text{scalp} \langle L_{\text{scalp}} \rangle + \Delta \mu_a \text{skull} \langle L_{\text{skull}} \rangle \\ & + \Delta \mu_a \text{CSF} \langle L_{\text{CSF}} \rangle + \Delta \mu_a \text{gray matter} \langle L_{\text{gray matter}} \rangle \\ & + \Delta \mu_a \text{white matter} \langle L_{\text{white matter}} \rangle. \end{aligned} \quad (2)$$

Assuming that only the absorption in the brain is changed by brain activation, i.e., $\Delta \mu_a \text{scalp} = \Delta \mu_a \text{skull} = \Delta \mu_a \text{CSF} = 0$ and $\Delta \mu_a \text{gray matter} = \Delta \mu_a \text{white matter} \equiv \Delta \mu_a \text{brain}$, the NIRS signal can be given by

$$\begin{aligned} \Delta OD & = \Delta \mu_a \text{brain} (\langle L_{\text{gray matter}} \rangle + \langle L_{\text{white matter}} \rangle) \\ & = \Delta \mu_a \text{brain} \langle L_{\text{brain}} \rangle, \end{aligned} \quad (3)$$

where $\Delta \mu_a \text{brain}$ is the absorption change in the brain and $\langle L_{\text{brain}} \rangle$ is the partial optical path length in the brain, which is shorter than the mean optical path length. The partial optical path length in the brain can be used as an index of the sensitivity of the NIRS signal to brain activation:

$$\frac{\partial OD}{\partial \mu_a \text{brain}} \approx \langle L_{\text{brain}} \rangle. \quad (4)$$

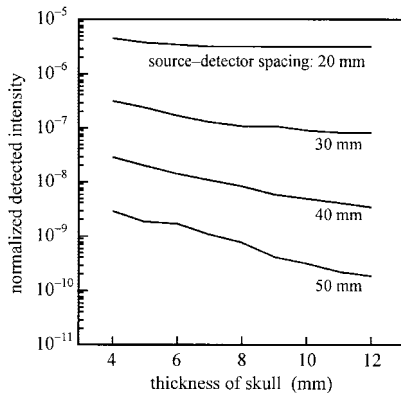


Fig. 2. Detected intensity for an adult head model as a function of skull thickness predicted by Monte Carlo simulation.

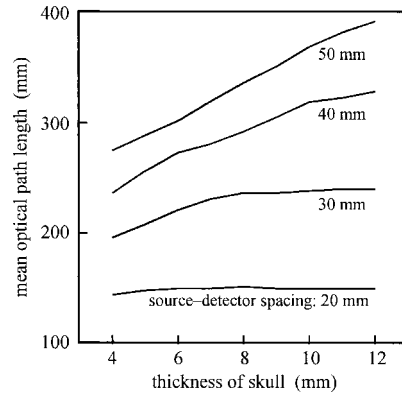


Fig. 3. Mean optical path length for an adult head model as a function of skull thickness predicted by Monte Carlo simulation.

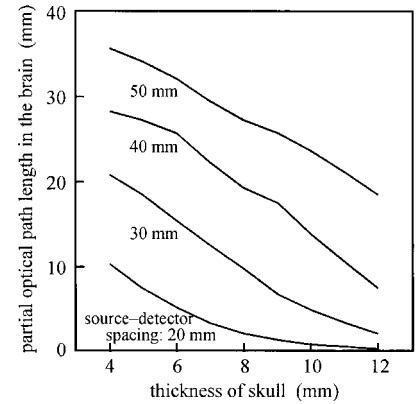


Fig. 4. Partial optical path length in the brain for an adult head model as a function of skull thickness predicted by Monte Carlo simulation.

The spatial sensitivity profile indicates the volume of tissue in which the absorption change contributes to the NIRS signal.⁷ The trajectories of the detected light can approximate the spatial sensitivity profile. The head model is divided into voxels, and the mean partial optical path length that the detected light travels within each voxel is calculated to obtain the trajectories of the detected light. The partial optical path length within a voxel $\langle L_{\text{voxel}}(x, y, z) \rangle$ approximates a partial derivative of the change in the detected intensity versus absorption coefficient in the voxel:

$$\frac{\partial OD}{\partial \mu_a \text{ voxel}(x, y, z)} \approx \langle L_{\text{voxel}}(x, y, z) \rangle. \quad (5)$$

In the results presented here, the partial optical path lengths within the voxels $\langle L_{\text{voxel}}(x, y, z) \rangle$ are projected onto the plane perpendicular to the boundaries of layers and along the source and detector (the x - z plane) and onto the plane parallel to the brain surface (the x - y plane) to represent two-dimensional distributions of the spatial sensitivity profile. The partial optical path length within the voxels in the gray matter and the white matter are projected onto the x - y plane to obtain topographic profiles of the spatial sensitivity to brain activation.

The light propagation in the model was calculated by use of a previously described Monte Carlo method⁶ based on a variance reduction technique.²⁰ Fifty million photons that initially have a unit survival weight were injected one by one into the source position. The propagation of a photon in the head model was determined from the transport scattering coefficient and random numbers. Isotropic scattering was assumed in all the layers. The scattering length was corrected when the photon crossed a boundary between different types of tissue. Reflection that is due to refractive-index mismatch was considered only on the boundary between the scalp and the air. The refractive indices of air and tissue were assumed to be 1.0 and 1.4, respectively. We

ignored the refractive-index mismatch between the CSF and the tissue because the refractive-index difference between the CSF and the tissue is less than that between the air and the tissue and the refractive-index mismatch between the CSF and the tissue has less of an effect on the light propagation in the brain than the scattering in the CSF layer caused by the arachnoid trabeculae.

When a photon reached the detector at 20, 30, 40, or 50 mm from the source, its ultimate survival weight W was calculated with absorption coefficient μ_{ai} and optical path length L_i that detected photon travel in each layer:

$$W = W_0 \exp \left[\sum (-\mu_{ai} L_i) \right], \quad (6)$$

where W_0 is the survival weight of the photon, reduced only by reflection at the surface of the model. The survival weight and partial optical path length in each layer weighted by the ultimate survival weight were recorded for each detector. The ultimate survival weight of the photons detected by each detector was accumulated to calculate the intensity of the detected light. The partial optical path length in each layer can be calculated by accumulation of the partial optical path lengths weighted by the ultimate survival weight for each detected photon. The mean optical path length is the sum of the partial optical path lengths. When the photon reached the detector at 30 mm from the source, the trajectory of the detected photon weighted by the ultimate weight was accumulated to obtain the spatial sensitivity profiles.

3. Results

A. Effect of Skull Thickness

The intensity of the detected light as a function of skull layer thickness is shown in Fig. 2. The detected intensity is normalized by the intensity of the incident light. The detected intensity slowly decreases with an increase in skull thickness. The

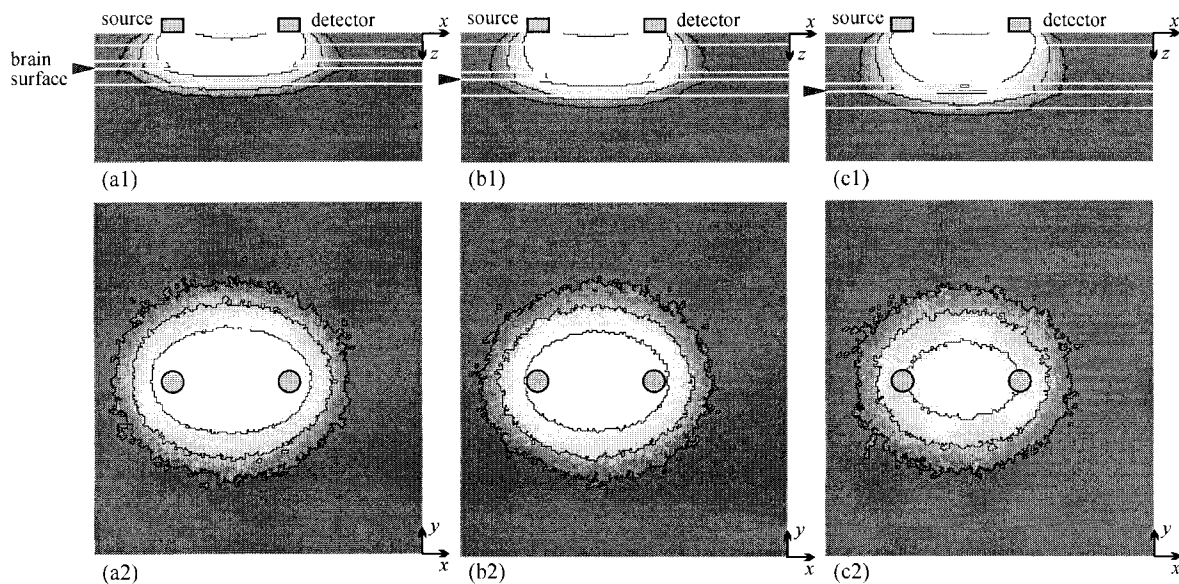


Fig. 5. Effect of skull thickness on spatial sensitivity profiles in the x - z and x - y planes. The skull thicknesses are (a) 4, (b) 7, (c) 10 mm.

slope increases with an increase in source–detector spacing. The detected intensity for a source–detector spacing of 30 mm is almost constant for a model with a skull thickness greater than 8 mm.

Figure 3 shows the mean optical path length as a function of skull layer thickness. The mean optical path length increases when the skull thickness increases. The slope for the larger source–detector spacings is greater than that for the small source–detector spacing. The slope for the source–detector spacing of 30 mm levels off when the skull is thicker than 8 mm. The mean optical path length for a source–detector spacing of 20 mm scarcely depends on skull thickness.

The relationship between the partial optical path length in the brain and the thickness of the skull is shown in Fig. 4. The partial optical path length decreases when the skull thickness increases. Although the partial optical path length for the small source–detector spacings levels off as zero separation

approaches, the slope is almost the same for the source–detector spacings that ranged from 20 to 50 mm. In the case of a source–detector spacing of 30 mm, the model with a 6-mm-thick skull has more than three times the partial optical path length in the brain compared with the model with a 10-mm-thick skull. This indicates that the sensitivity of the NIRS signal-to-brain activation is considerably affected by the thickness of the skull layer.

The spatial sensitivity profiles for the head model with skull layers of 4-, 7-, and 10-mm thickness at a source–detector spacing of 30 mm are shown in Figs. 5(a), 5(b), and 5(c), respectively. The gray scale of all the profiles is normalized by the maximum value in Fig. 5(b). The contours in all the profiles are drawn for 10%, 1%, and 0.1% with respect to the maximum sensitivity point in Fig. 5(b). As shown in the spatial sensitivity profiles in the x - z plane (Figs. 5(a1), 5(b1), and 5(c1)), deeper penetration from the head surface is observed in the model with a thicker skull although penetration into the brain surface decreases slightly with an increase in skull thickness. The most intense region of the spatial sensitivity profile in the x - y plane in the brain is reduced and is concentrated at the midpoint of the source and detector with an increase in skull thickness, as shown in Figs. 5(a2), 5(b2), and 5(c2). The position of the extreme contours scarcely depends on the thickness of the skull. Figure 6 shows the profile of the spatial sensitivity profile in the brain along the y axis at the midpoint of the source and detector. The sensitivity peak decreases with an increase in skull thickness whereas the full width at half-maximum (FWHM) of the profile scarcely depends on the thickness of the skull. The FWHM of the spatial sensitivity profile on the y axis at the midpoint of the source and detector for a source–detector spacing of 30 mm is approximately 15 mm.

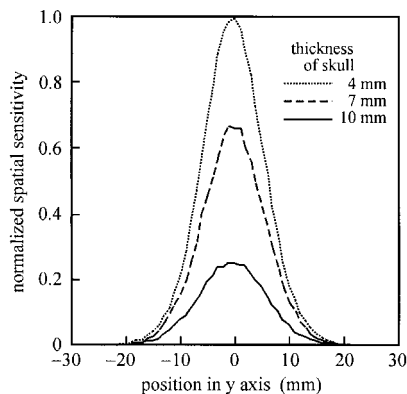


Fig. 6. Effect of skull thickness on the profile of the spatial sensitivity profile in the brain along the y axis at the midpoint of the source and the detector.

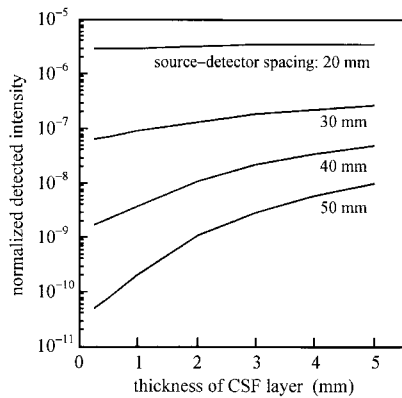


Fig. 7. Detected intensity for an adult head model as a function of the CSF layer thickness predicted by Monte Carlo simulation.

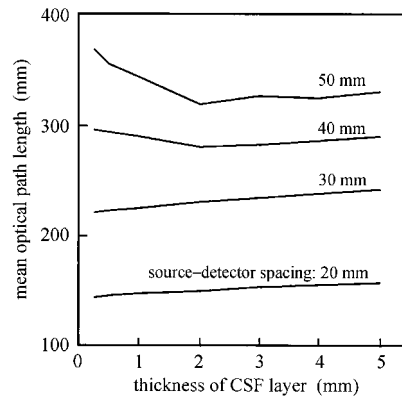


Fig. 8. Mean optical path length for an adult head model as a function of the CSF layer thickness predicted by Monte Carlo simulation.

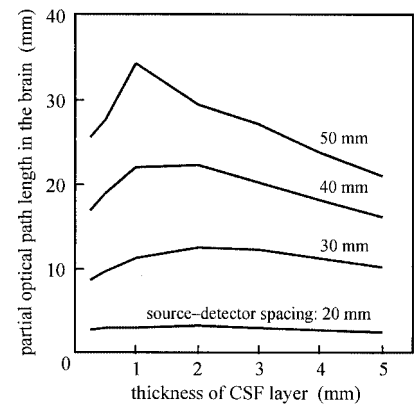


Fig. 9. Partial optical path length in the brain for an adult head model as a function of the CSF layer thickness predicted by Monte Carlo simulation.

B. Effect of the Cerebrospinal Fluid Layer Thickness

The effect of the CSF layer thickness on the intensity of the detected light is shown in Fig. 7. The detected intensity increases with increased thickness of the CSF layer but the slope becomes more gradual in the case of thick CSF layers. The slope decreases with a decrease in source–detector spacing, and the detected intensity for a source–detector spacing of 20 mm scarcely depends on the thickness of the CSF.

The relationship between the mean optical path length and the source–detector spacing is shown in Fig. 8. The mean optical path length for source–detector spacings of 40 and 50 mm initially decreases with an increase in CSF thickness up to 2 mm whereas it increases slightly with an increase in the CSF layer thickness beyond 2 mm. The mean optical path length for source–detector spacings of 20 and 30 mm increases slightly when the thickness of the CSF increases. The slope for all the source–detector spacing is almost the same beyond a CSF thickness of 2 mm.

Figure 9 shows the partial optical path length as a function of the thickness of the CSF layer. The partial optical path length initially increases when the CSF layer thickness increases, then starts to decrease with additional increases in CSF layer thickness. A marked peak can be observed for a large source–detector spacing. The thickness of the CSF layer for which the partial optical path length reaches its peak decreases when the source–detector spacing increases. The difference in the partial optical path length caused by the thickness of the CSF is not significant for a source–detector spacing of 20 mm. In the case of a source–detector spacing of 30 mm, the partial optical path length for the head model with a 2-mm-thick CSF layer is approximately 20% longer than that for a head model with a 5-mm thick CSF layer.

The spatial sensitivity profiles for head models with CSF layers of 0.5-, 3-, and 5-mm thickness at a source–detector spacing of 30 mm are shown in Fig. 10. The gray scale of all the profiles is normalized by the maximum value in Fig. 5(b) and the contours in all the profiles are drawn for 10%, 1%, and 0.1% with

respect to the maximum sensitivity point in Fig. 5(b) to allow one to compare the effect of the thickness of the CSF on the spatial sensitivity profiles with those computed for the effect of the thickness of the skull. A deeper penetration of the spatial sensitivity profile from the head surface can be observed in the models with thicker CSF layers as shown in Figs. 10(a1), 10(b1), and 10(c1). The penetration depth into the brain surface scarcely depends on the thickness of the CSF layer. Both the maximum intensity region and the extreme contours of the spatial sensitivity profile in the x - y plane in the brain are broadened when the thickness of the CSF layer increases as shown in Figs. 10(a2), 10(b2), and 10(c2). Figure 11 shows the profile of the spatial sensitivity in the brain along the y axis at the midpoint of the source and detector. The sensitivity peak decreases when the CSF layer thickness increases. The side of the profile spreads considerably when the thickness of the CSF layer increases whereas the FWHM of the profile scarcely depends on the thickness of the CSF layer and is approximately 15 mm.

4. Discussion

The brain can move or expand to a limited degree in the skull, and it is possible that the thickness of the CSF varies during the NIRS measurements or because of changes in posture. Since changes in the thickness of the CSF layer alter the intensity of detected light as shown in Fig. 7, any brain movement and expansion during the measurement would affect the NIRS signal. This phenomenon has been briefly discussed by Firbank *et al.*¹³

The thickness of the skull and the CSF varies with position around the head and between individuals even if the thickness does not change during the measurement. The sensitivity of the NIRS signal to change in brain activity is thus likely to depend on the depth of the brain surface from the surface of the head. The partial optical path length in the brain is one of the important parameters required to estimate the effect of the thickness of the superficial layers on

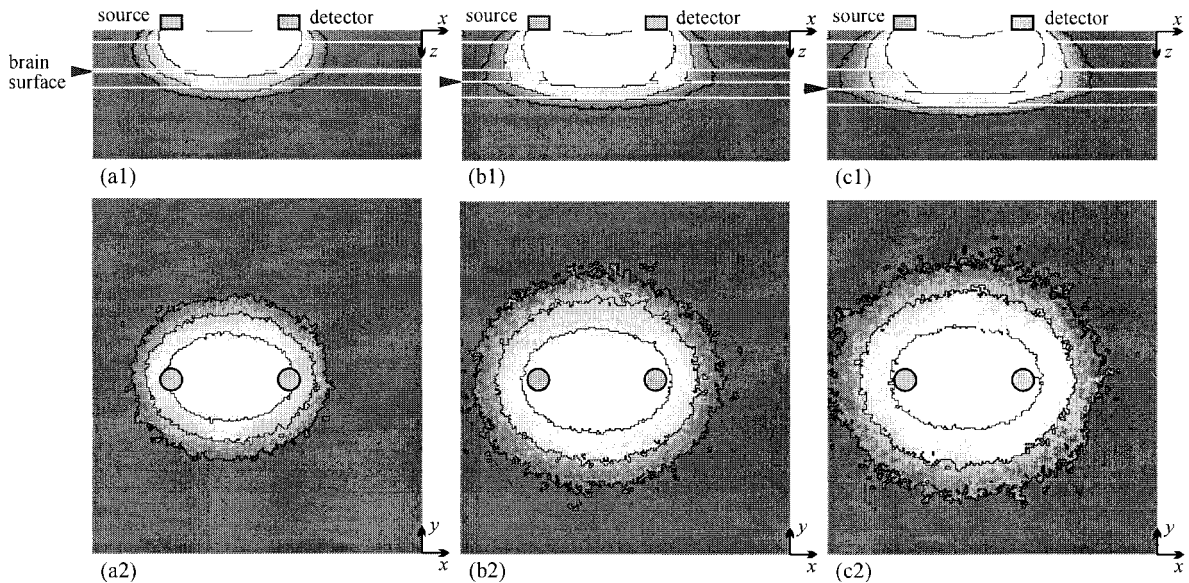


Fig. 10. Effect of the CSF layer thickness on the spatial sensitivity profiles in the x - z and the x - y planes. The CSF thicknesses are (a) 0.5, (b) 3, (c) 5 mm.

the sensitivity of the NIRS signal-to-brain activation. As can be seen in Figs. 4 and 9, the partial optical path length in the brain for a source–detector spacing of 30 mm depends to a great extent on the thickness of the skull whereas the thickness of the CSF layer scarcely affects the partial optical path length in the brain. These results suggest that the sensitivity of the NIRS signal-to-brain activation for small source–detector spacings depends mainly on the depth of the inner surface of the skull rather than the depth of the brain surface. For example, the depth of the brain from the head surface for a head model with a skull layer of 7 mm and a CSF layer of 5 mm is the same as that for a head model with a skull layer of 10 mm and a CSF layer of 2 mm. The partial optical path length for the former model is more than twice as long as that for the latter model. The sensitivity of the NIRS signal for the large source–detector spacing is

affected by both the depth of the inner surface of the skull and the thickness of the CSF layer.

Since the partial optical path length in the brain is based on the assumption that the absorption in the brain is homogeneously changed by brain activation, it cannot be directly applied to evaluate the sensitivity of the NIRS signal for local brain activation. As can be seen from Figs. 10 and 11, the spatial sensitivity profile is broadened when the CSF layer thickness increases. The sensitivity at the midpoint of the source and detector for the model with a 5-mm-thick CSF layer is approximately half of that for a model with a 0.5-mm-thick CSF layer whereas the partial optical path length in the brain for the two models is almost the same. These results suggest that the sensitivity of the NIRS signal to the local brain activation depends on not only the depth of the inner skull but also the thickness of the CSF layer.

The spatial sensitivity profile depends on both the depth of the inner skull and the thickness of the CSF layer as well as the partial optical path length in the brain and, hence, cannot be predicted from only the depth of the brain surface. As can be seen in Figs. 5(c) and 10(c), the spatial sensitivity profile for a head model with a skull layer of 7 mm and a CSF layer of 5 mm is distributed more broadly in the brain than that for a model with a skull of 10 mm and a CSF layer of 2 mm although the depth of the brain surface for the two head models is the same. The spatial sensitivity profile in the x - y plane indicates the volume of tissue interrogated by a source–detector pair for topographic imaging. Since the thickness of the skull and CSF layers varies with position on the head, the sensitivity and interrogated region for individual source–detector pairs for topographic imaging can differ from each other.

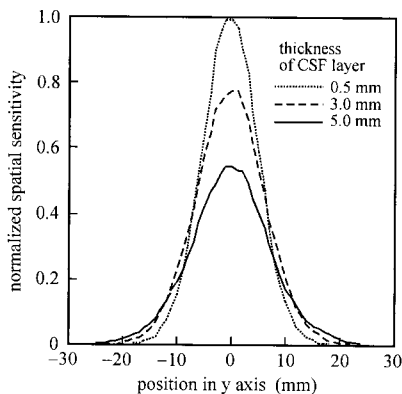


Fig. 11. Effect of the CSF thickness on the spatial sensitivity profile in the brain along the y axis at the midpoint of the source and the detector.

Although the partial optical path length and the spatial sensitivity profiles in the brain are important parameters as indices of the sensitivity of the NIRS signal-to-brain activation, they cannot be directly measured *in vivo* and thus have to be predicted from numerical modeling of light propagation in the head. The mean optical path length has frequently been used to determine the induced change of oxyhemoglobin and deoxyhemoglobin in the brain as an alternative to the partial optical path length in the brain because the mean optical path length can be measured by time- or phase-resolved instrumentation. It should be noted that the mean optical path length increases when the skull thickness increases as shown in Fig. 3 whereas the partial optical path length decreases when the skull thickness increases as shown in Fig. 4. The effect of the CSF layer thickness also has this contrasting tendency between the mean optical path length and the partial optical path length as shown in Figs. 8 and 9. These results indicate that it is not appropriate to use the mean optical path length as an alternative to the partial optical path length in the brain to compensate for the differences in sensitivity caused by the thickness variation of the superficial tissue layers in the head. In NIRS and imaging, differences in optical path length cause a cross talk between oxyhemoglobin and deoxyhemoglobin.¹² An image reconstruction algorithm^{21,22} that predicts the path length in the activated region of the brain might reduce the cross talk in the measurement more effectively than a calculation by use of the mean optical path length.

5. Conclusion

The effect of the thickness of the skull and CSF layer on light propagation in the brain in an adult head model has been investigated by Monte Carlo simulation. Changes in the CSF thickness caused by brain movement and/or expansion during measurements significantly affect the intensity of the detected light, i.e., the NIRS signal. The partial optical path length in the brain, i.e., the sensitivity of the NIRS signal to the global absorption change in the brain, depends mainly on the depth of the inner skull below the surface and scarcely depends on the thickness of the CSF layer for a source–detector spacing of 30 mm, which is commonly used for near-infrared topographic imaging. However, the spatial sensitivity profile that indicates the volume of tissue interrogated by a source–detector pair is broadened when the thickness of the CSF layer increases. The sensitivity at the midpoint of the source and detector decreases when the CSF layer thickness increases whereas the partial optical path length in the brain is almost the same. The sensitivity of the NIRS signal to local brain activation therefore depends on not only the depth of the inner skull but also the thickness of the CSF layer.

The mean optical path length increases slightly when the skull thickness increases whereas the partial optical path length decreases. This contrasting tendency is also observed in the effect of the CSF

layer on the mean optical path length and the partial optical path length. It is therefore not appropriate to use the mean optical path length as an alternative to the partial optical path length to compensate for the difference in sensitivity caused by thickness variations of the superficial tissue layers in the head.

This research was partly supported by the Japan Society for the Promotion of Science, Grants-in-Aid for Scientific Research 13558116 and 13750397, a research grant from the Okawa Foundation for Information and Telecommunications, and a research grant from the Casio Science Promotion Foundation.

References

1. R. Springett, M. Wylezinska, E. B. Cady, M. Cope, and D. T. Delpy, "Oxygen dependency of cerebral oxidative phosphorylation in newborn piglets," *J. Cereb. Blood Flow Metab.* **20**, 280–289 (2000).
2. S. Kohri, Y. Hoshi, M. Tamura, C. Kato, Y. Kuge, and N. Tamaki, "Quantitative evaluation of the relative contribution ratio of cerebral tissue to near-infrared signals in the adult human head: a preliminary study," *Physiol. Meas.* **23**, 301–312 (2002).
3. A. Maki, Y. Yamashita, Y. Ito, E. Watanabe, Y. Mayanagi, and H. Koizumi, "Spatial and temporal analysis of human motor activity using noninvasive NIR topography," *Med. Phys.* **22**, 1997–2005 (1995).
4. T. Yamamoto, A. Maki, T. Kadoya, Y. Tanikawa, Y. Yamada, E. Okada, and H. Koizumi, "Arranging optical fibers for the spatial resolution improvement of topographic images," *Phys. Med. Biol.* **47**, 3429–3440 (2002).
5. B. Chance, E. Anday, S. Nioka, S. Zhou, L. Hong, K. Worden, C. Li, T. Murray, Y. Ovetsky, D. Pidikiti, and R. Thomas, "A novel method for fast imaging of brain function, non-invasively, with light," *Opt. Express* **2**, 411–423 (1998), <http://www.opticsexpress.org>.
6. M. Hiraoka, M. Firbank, M. Essenpreis, M. Cope, S. R. Arridge, P. van der Zee, and D. T. Delpy, "A Monte Carlo investigation of optical pathlength in inhomogeneous tissue and its application to near-infrared spectroscopy," *Phys. Med. Biol.* **38**, 1859–1876 (1993).
7. E. Okada, M. Firbank, and D. T. Delpy, "The effect of overlying tissue on the spatial sensitivity profile of near-infrared spectroscopy," *Phys. Med. Biol.* **40**, 2093–2108 (1995).
8. E. Okada, M. Firbank, M. Schweiger, S. R. Arridge, M. Cope, and D. T. Delpy, "Theoretical and experimental investigation of near-infrared light propagation in a model of the adult head," *Appl. Opt.* **36**, 21–31 (1997).
9. M. Firbank, S. R. Arridge, M. Schweiger, and D. T. Delpy, "An investigation of light transport through scattering bodies with nonscattering regions," *Phys. Med. Biol.* **41**, 767–783 (1996).
10. M. Wolf, M. Keel, V. Dietz, K. von Siebenthal, H. U. Bucher, and O. Baenziger, "The influence of a clear layer on near-infrared spectrophotometry measurements using a liquid neonatal head phantom," *Phys. Med. Biol.* **44**, 1743–1753 (1999).
11. H. Dehghani, S. R. Arridge, M. Schweiger, and D. T. Delpy, "Optical tomography in the presence of void regions," *J. Opt. Soc. Am. A* **17**, 1659–1670 (2000).
12. K. Uludag, M. Kohl, J. Steinbrink, H. Obrig, and A. Villringer, "Cross talk in the Lambert–Beer calculation for near-infrared wavelength estimated by Monte Carlo simulation," *J. Biomed. Opt.* **7**, 51–59 (2002).
13. M. Firbank, E. Okada, and D. T. Delpy, "A theoretical study of the signal contribution of regions of the adult head to near-infrared spectroscopy studies of visual evoked responses," *Neuroimage* **8**, 69–78 (1998).

14. J. Plucinski, A. F. Frydrychowski, J. Kaczmarek, and W. Juzwa, "Theoretical foundations for noninvasive measurement of variations in the width of the subarachnoid space," *J. Biomed. Opt.* **5**, 291–299 (2000).
15. C. R. Simpson, M. Kohl, M. Essenpreis, and M. Cope, "Near-infrared optical properties of *ex vivo* human skin and subcutaneous tissue measured using the Monte Carlo inversion technique," *Phys. Med. Biol.* **43**, 2465–2478 (1998).
16. M. Firbank, M. Hiraoka, M. Essenpreis, and D. T. Delpy, "Measurement of the optical properties of the skull in the wavelength range 650–950 nm," *Phys. Med. Biol.* **38**, 503–510 (1993).
17. P. van der Zee, M. Essenpreis, and D. T. Delpy, "Optical properties of brain tissue," in *Photon Migration and Imaging in Random Media and Tissues*, R. R. Alfano and B. Chance, eds., *Proc. SPIE* **1888**, 454–465 (1993).
18. E. Okada and D. T. Delpy, "Near-infrared light propagation in an adult head model. I. Modeling of low-level scattering in the cerebrospinal fluid layer," *Appl. Opt.* **42**, 2906–2914 (2003).
19. D. T. Delpy, M. Cope, P. van der Zee, S. R. Arridge, S. Wray, and J. Wyatt, "Estimation of optical pathlength through tissue from direct time of flight measurement," *Phys. Med. Biol.* **33**, 1433–1442 (1988).
20. B. C. Wilson, "A Monte Carlo model for the absorption and flux distribution of light in tissue," *Med. Phys.* **10**, 824–830 (1983).
21. S. R. Arridge and J. C. Hebden, "Optical imaging in medicine. II. Modelling and reconstruction," *Phys. Med. Biol.* **42**, 841–853 (1997).
22. D. A. Boas, T. Gaudette, G. Strangman, X. Cheng, J. J. A. Marota, and J. B. Mandeville, "The accuracy of near infrared spectroscopy and imaging during focal changes in cerebral hemodynamics," *Neuroimage* **13**, 76–90 (2001).